FINAL REPORT FOR AFOSR
GRANT NO. F49620-92-J-0089:

"Ultraviolet and Visible Lasers: Rare Earth-Doped Waveguide Devices and Non-Linear Optical Extraction Techniques"

Period:
December 1, 1991 – November 30, 1994

Prepared for
Dr. H. R. Schlossberg
Physics and Electronics Directorate
AFOSR/NE
Bolling AFB
Washington, DC 20032

Submitted by
J. G. Eden
Department of Electrical and Computer Engineering
University of Illinois
Urbana-Champaign Campus
1406 West Green Street
Urbana, IL 61801

December 1994

REPORT DOCUMENTATION PAGE

Form Approved
OMB No 0704-0188

1. AGENCY USE ONLY (Leave blank)	2. REPORT DATE	3. REPORT TYPE AND DATES COVERED
		FINAL REPORT

4. TITLE AND SUBTITLE
ULTRAVIOLET AND VISIBLE LASERS: RARE EARTH-DOPED WAVEGUIDE DEVICES AND NON-LINEAR OPTICAL EXTRACTION TECHNIQUES

5. FUNDING NUMBERS
61102F
2301/CS

6. AUTHOR(S)
Prof J. G. Eden

7. PERFORMING ORGANIZATION NAME(S) AND ADDRESS(ES)
Dept of Electrical and Computer Engineering
Univ of Illinois
Urbana-Champaign Campus
1406 West Green Street
Urbana, IL 61801

8. PERFORMING ORGANIZATION REPORT NUMBER
AFOSR-TR- 95-0321

9. SPONSORING/MONITORING AGENCY NAME(S) AND ADDRESS(ES)
AFOSR/NE
110 Duncan Avenue Suite B115
Bolling AFB DC 20332-0001

10. SPONSORING/MONITORING AGENCY REPORT NUMBER
F49620-92-J-0089

11. SUPPLEMENTARY NOTES

12a. DISTRIBUTION/AVAILABILITY STATEMENT
APPROVED FOR PUBLIC RELEASE: DISTRIBUTION UNLIMITED

13. ABSTRACT (Maximum 200 words)

SEE FINAL REPORT ABSTRACT

14. SUBJECT TERMS	15. NUMBER OF PAGES
	16. PRICE CODE

17. SECURITY CLASSIFICATION OF REPORT	18. SECURITY CLASSIFICATION OF THIS PAGE	19. SECURITY CLASSIFICATION OF ABSTRACT	20. LIMITATION OF ABSTRACT
UNCLASSIFIED	UNCLASSIFIED	UNCLASSIFIED	UNCLASSIFIED

I. INTRODUCTION

Over the past three years, AFOSR has supported a combined experimentalersity of Illinois that has focused on the demonstration and development of new coherent sources operating in the ultraviolet and short wavelength portion of the visible (green → violet). This research effort has two thrusts. Emphasis is being placed on the demonstration of fiber and planar waveguide lasers based upon upconversion processes in rare earth-doped glasses. These devices have several attractive features for applications in communications, reprographics and medicine (in particular), including: 1) wide tunability (several nm), 2) broad absorption spectra suitable for diode laser pumping, 3) overall efficiencies exceeding 10% despite the required absorption of at least two pump photons, 4) pump-gain medium interaction lengths not normally available with bulk crystals, 5) the ability to integrate planar waveguide glass-based lasers with other devices such as EO-modulators and laser diodes, and 6) multiple wavelengths and high quantum efficiencies (> 50%).

To date, much of our effort has been centered on examining the upconversion (or the sequential absorption of two pump photons) of Ho^{3+} or Nd^{3+} ions in fluorozirconate glass (ZBLAN) fibers and several significant accomplishments have been realized:

1) Lasing in the ultraviolet (381 nm) and violet (412 nm) has been obtained from Nd-doped ZBLAN fibers. This is the first demonstration of an ultraviolet fiber laser pumped by any means.
2) The Ho:ZBLAN fiber laser (λ ~ 546-550 nm) has been extensively characterized with respect to fiber length (20-90 cm), output coupling and pump power. Output powers exceeding 38 mW have been obtained for an absorbed pump power of 280 mW at room temperature. Slope and overall efficiencies of 24% and > 13%, respectively, are obtained reproducibly for an output coupling of 30%. This laser has been continuously tuned over more than 5 nm

and multi-line operation has been effectively suppressed. Several emission and small signal gain and absorption measurements have also been conducted.

3) Laser ablative deposition of fluorozirconate glass films has been demonstrated with an ArF laser. Also, a new two-step process for diffusing silver into bulk ZBLAN glass has been tested successfully. This portion of the effort is devoted to fabricating planar waveguides.

4) Spectroscopic studies of other rare earth:ZBLAN fibers (notably Nd:ZBLAN and Pr:ZBLAN) have been carried out with the motivation of identifying potential lasing transitions having wavelengths below 450 nm.

5) As part of a collaborative program with NIST (Boulder, CO), we are analyzing the characteristics of Er-doped $LiTaO_3$ waveguides produced by Ti in-diffusion. These devices emit strongly in the green and are suitable for on-chip integration as modulated lasers.

In addition to these experiments, we have been pursuing several gas phase schemes for generating tunable, coherent radiation in the deep UV and VUV. Results that we have been working towards for several years have been realized. Specifically:

1) We have demonstrated an anti-Stokes Raman amplifier based on a small molecule in which a low-lying metastable state serves as the storage (initial) level. Gain on the $GO_u^+ \rightarrow XO_g^+$ band of Hg_2 in the deep UV ($\lambda \sim 225$ nm) has been observed in an anti-Stokes (stimulated electronic Raman scattering) scheme in which the metastable AO_g^+ excited state of the dimer serves as the storage level. A yellow photon drives the $G \leftarrow A$ transition and the magnitude and spectral dependence of the gain in the UV are in agreement with theoretical estimates.

2) Coherent radiation in the visible and UV (321-404 nm) has been obtained by a four wave parametric process in potassium vapor driven by femtosecond pulses (~ 80 fs). This single color pumping scheme ($2\omega_1 - \omega_2$) yields beams of high

spatial coherence and appears to be an efficient mechanism for generating pulses in the UV.

Each of these results is described in more detail in the next section.

II. ACCOMPLISHMENTS REALIZED UNDER AFOSR F49620-92-J-0089 SUPPORT

A. Ultraviolet and Violet Lasers in Nd:ZBLAN Fibers

This past summer, two of my graduate students obtained lasing in the ultraviolet (381 nm) from neodymium-doped ZBLAN fibers. Two months later, they were able to obtain oscillation on a violet transition. In several ways, these results represent the culmination of two years of spectroscopic studies of rare earth-doped ZBLAN fibers. Both lasers constitute a major step forward in fiber laser development for several reasons: 1) The 381 nm Nd:ZBLAN laser is the first UV fiber laser – this device promises to have several applications in reprographics, medicine and lithography, 2) both the 381 and 412 nm Nd:ZBLAN lasers are the shortest wavelength fiber laser transitions demonstrated to date; said another way, they extend the photon energies available from room temperature fiber lasers by roughly 0.6 eV, and 3) these transitions are the first lasing lines to have been pumped by upconversion in an Nd-doped fiber.

The fluorescence and laser spectra for the UV transition are shown in Fig. 1. The spontaneous emission profile has a FWHM of ~ 5 nm, but when two highly-reflecting mirrors are butt-coupled to the fiber, the spectrum collapses to a linewidth $< 10^{-2}$ nm. Lasing occurs at 381 nm and the beam is easily seen in normal room light with the aid of a card and, with < 0.1% of cavity output coupling, 74 μW of power is obtained for 275 mW of pump power. For this value of output coupling, the laser's slope efficiency is only ~ 0.1-0.2% but higher output couplings (which have not yet been investigated) will undoubtedly improve the device's overall efficiency. At present, this laser is pumped by the absorption of two photons in the orange (~ 590 nm). Several two color experiments

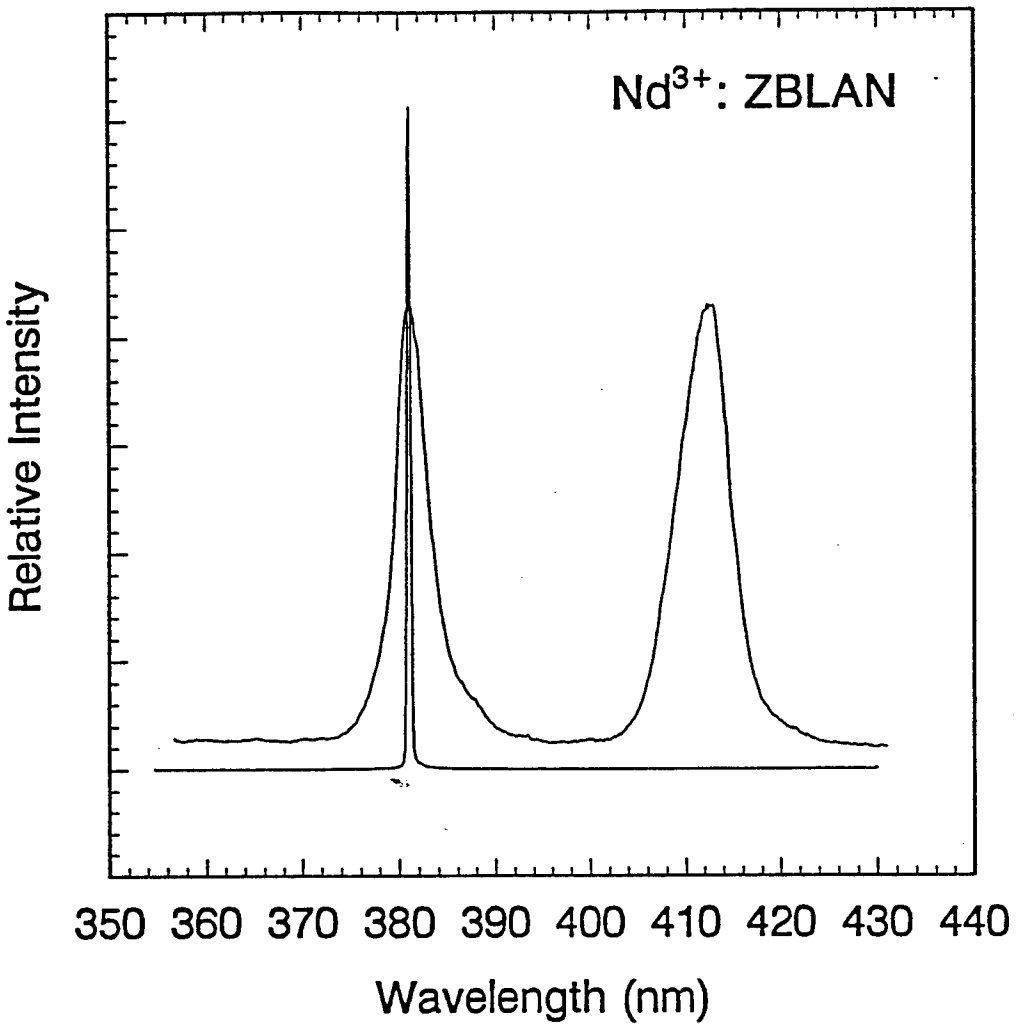

Figure 1 Fluorescence and laser spectra for the UV (381 nm) line in Nd:ZBLAN fibers.

have also been conducted involving one deep red ($\lambda > 680$ nm) and one near-infrared photon and the results suggest that diode laser pumping of this laser should be feasible.

Figure 2 shows the spontaneous emission and laser spectra for the 412 nm Nd:ZBLAN transition. For these experiments, the only output coupling studied to date is 0.4% and Fig. 3 gives the output power data obtained. Note that threshold occurs for ~ 225 mW incident on the fiber (the measured launch efficiency is < 35%) and the slope efficiency is ~ 0.5% for a 39 cm long fiber. We expect that, with increased cavity output coupling, the slope efficiency will exceed 5% and the overall efficiency several percent.

The excitation spectrum for the violet laser (obtained by measuring the output power as the pump wavelength was varied) of Fig. 4 reveals that, although lasing is most intense when the pump wavelength lies between 587 and 592 nm, the breadth of the excitation spectrum is > 10nm! The modulation superimposed onto the spectrum is a result of variations in pump power because of reflections from the optics responsible for coupling the pump to the fiber. Figures 5 and 6 illustrate the temporal behavior of the violet laser (note that Fig. 6 gives an expanded time base). Spiking of the laser waveform is observed immediately after the pump is initiated. However, the spiking decays quickly (has vanished after ~ 250 μs) and true CW operation is observed thereafter.

In summary, although the development of these new UV and violet lasers is still in the early stages, they show considerable promise as compact sources of tunable radiation in a spectral region that is an attractive one for DOD applications in microelectronics, patterning for materials processing, and medicine.

B. Lasing in Ho:ZBLAN Glass Fibers

Much of the effort under this program has been devoted to examining the behavior and key physical mechanisms responsible for lasing in fluorozirconate glass fibers and most of the goals set forth in our original proposal three years ago have been realized.

The Ho:ZBLAN fiber laser (λ ~ 546-550 nm) has been studied extensively and characterized with respect to fiber length, output coupling and pump wavelength. For

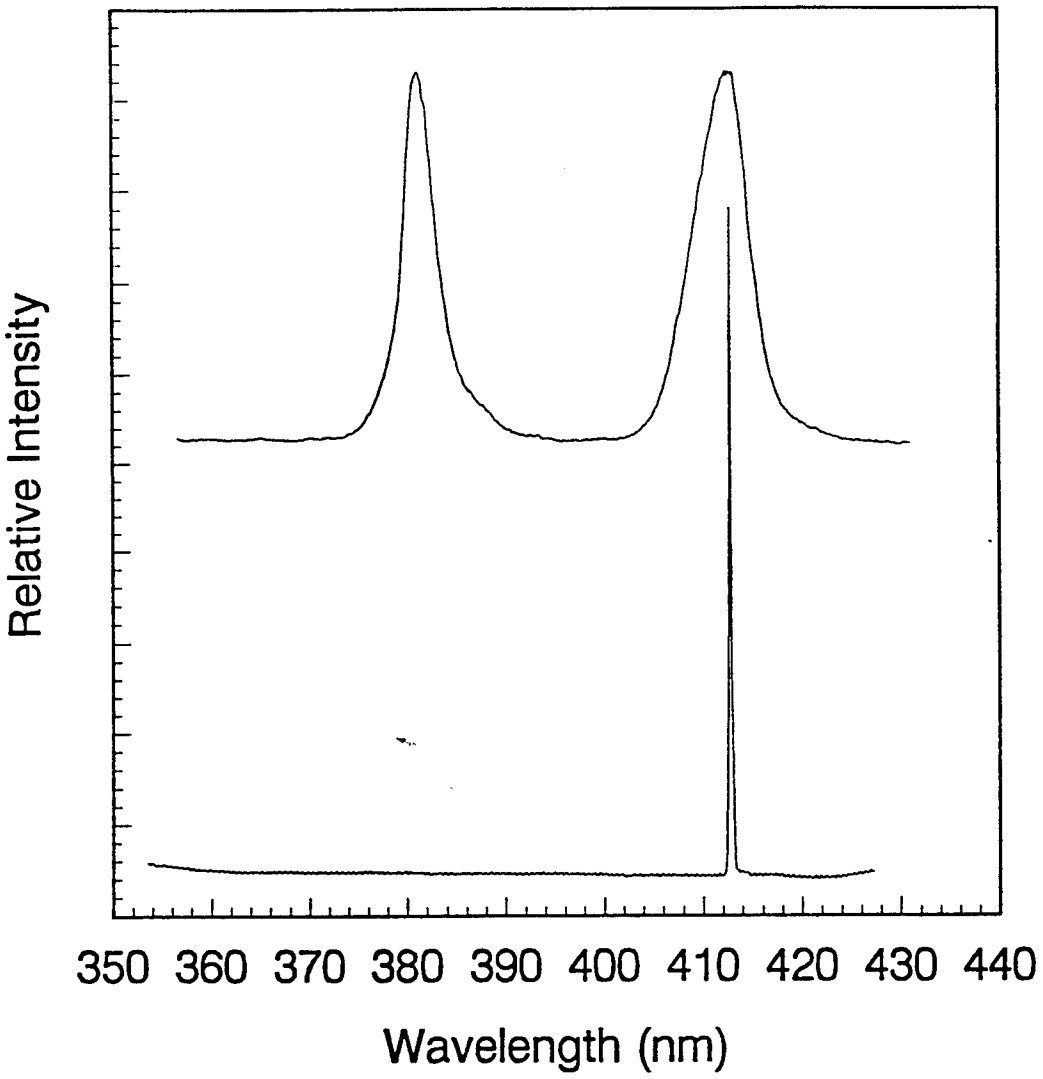

Figure 2 Spontaneous emission (top) and laser spectra for the violet transition of Nd^{3+} in ZBLAN fibers.

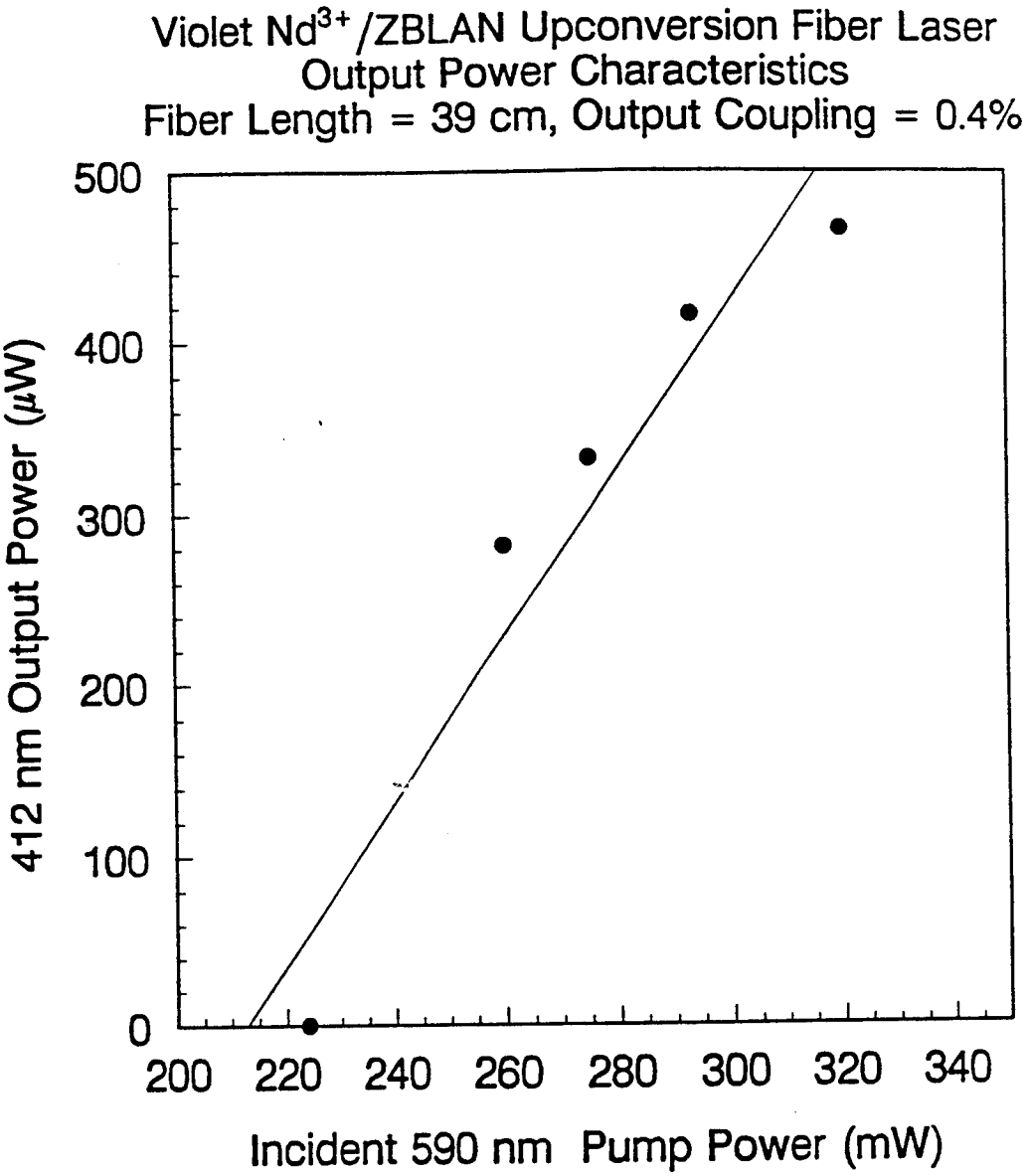

Figure 3 Dependence of output power on incident pump power for the violet fiber laser. The solid line represents a slope efficiency of 0.4%.

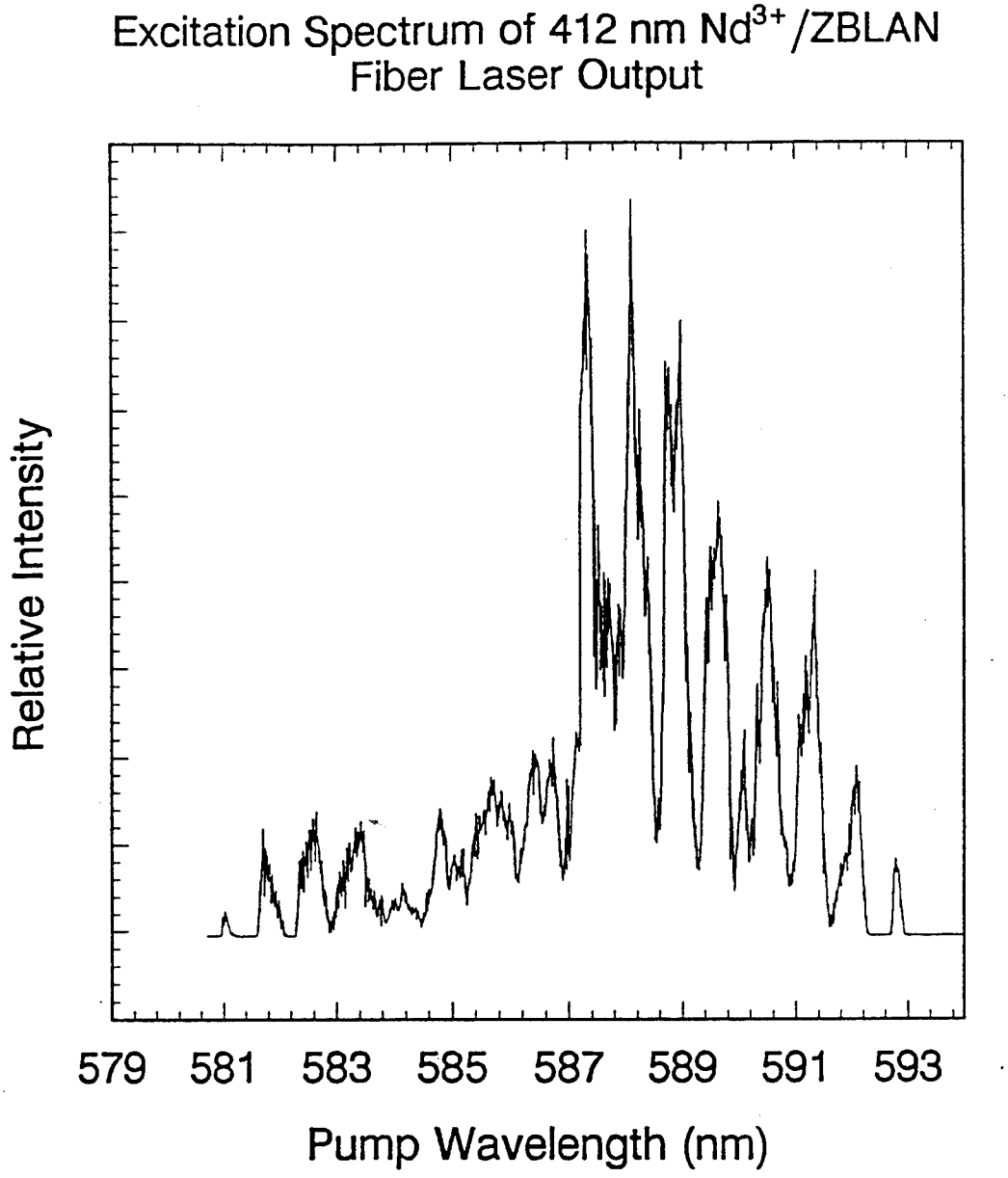

Figure 4 Excitation spectrum for the Nd:ZBLAN violet fiber laser.

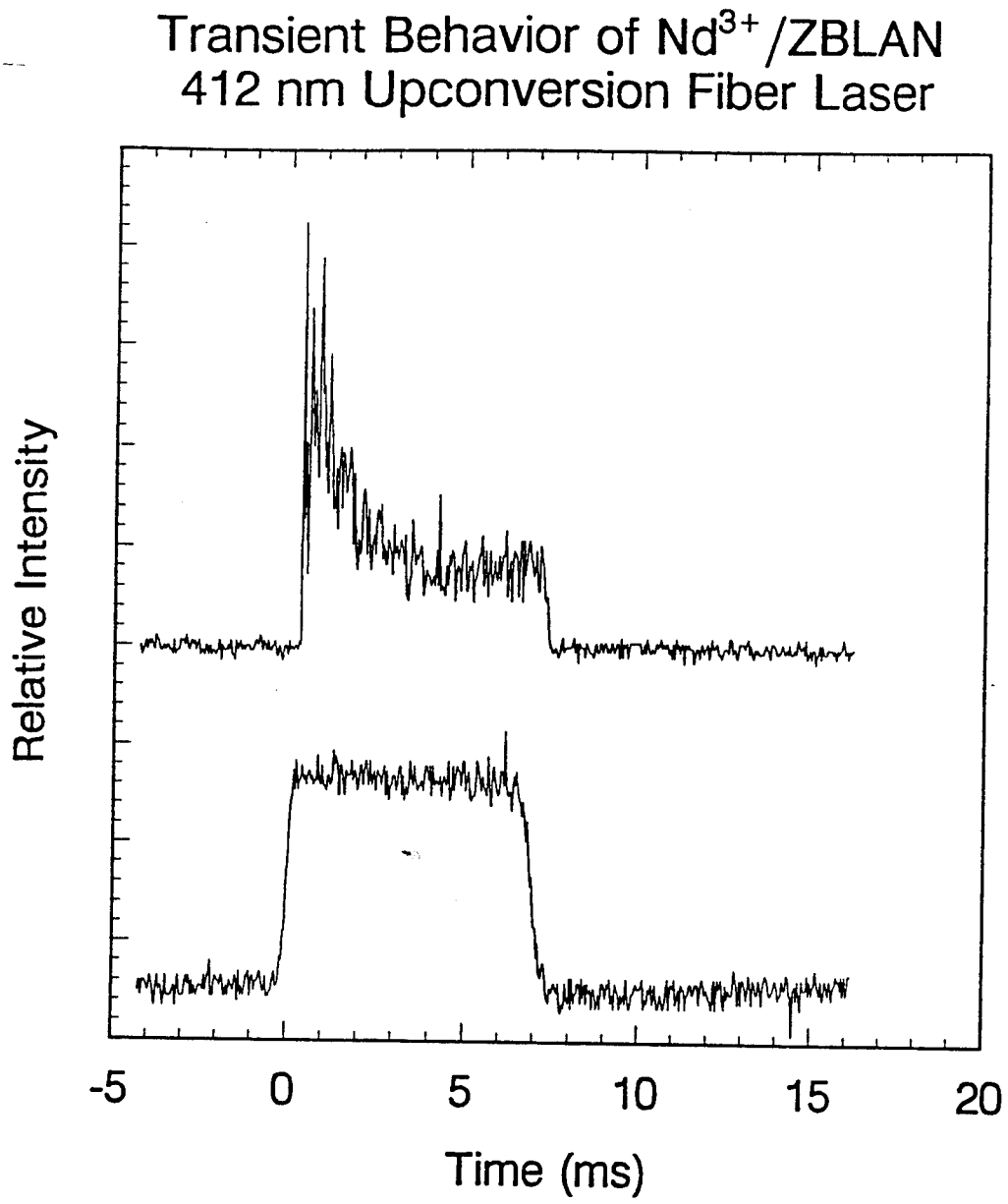

Figure 5 Laser (top) and pump waveforms for the Nd:ZBLAN violet (412 nm) transition.

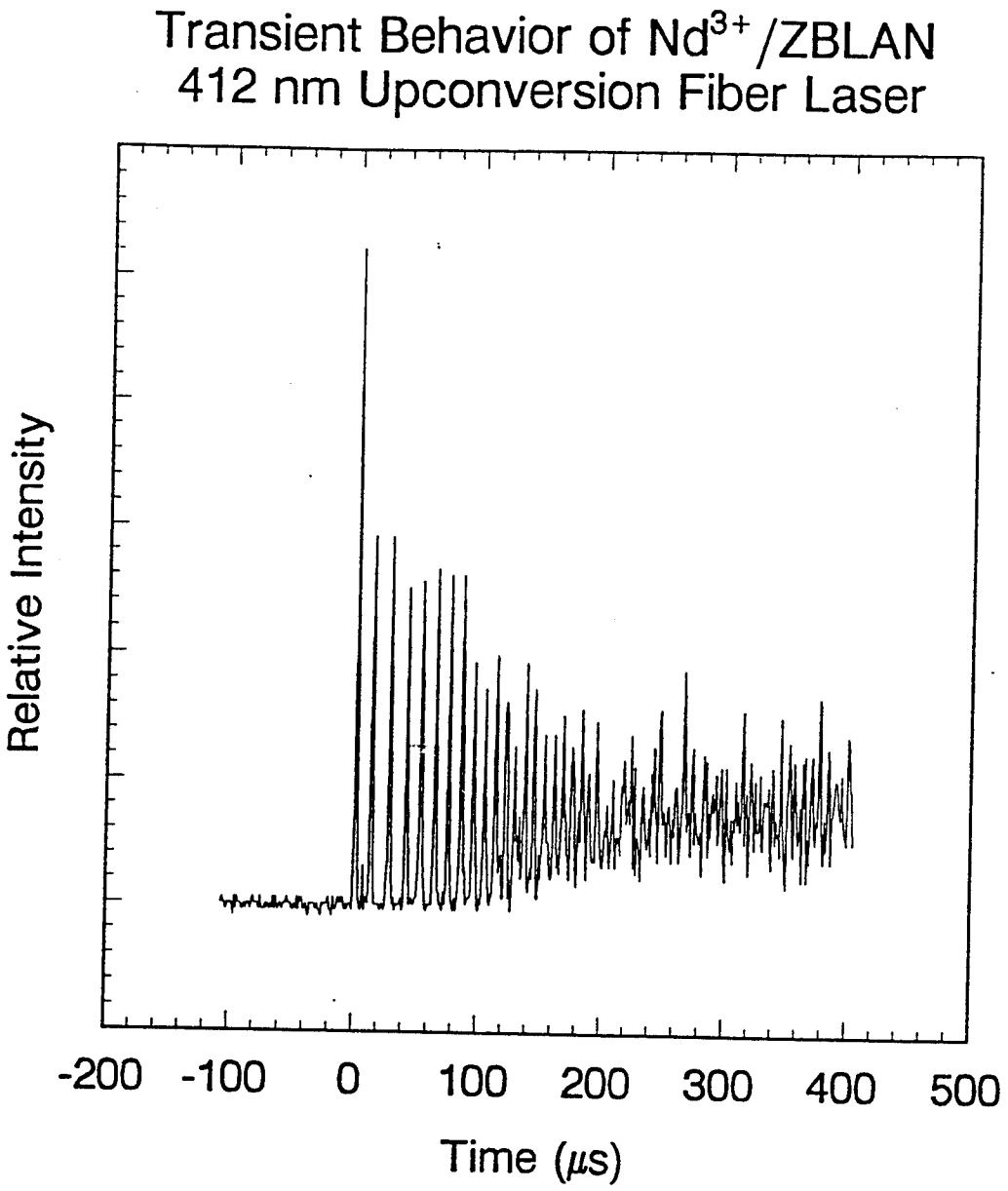

Figure 6 Expanded view of the violet laser waveform showing spiking for the first 200-300 μs.

example, Figs. 7 and 8 show the dependence of the Ho:ZBLAN laser's output power on cavity coupling for two different lengths of fiber (21 and 86 cm, respectively). For the shorter fiber, output powers of almost 40 mW have been obtained at room temperature for an output coupling of 30%. The intriguing aspect of these data is that the output power shows no signs of saturating with respect to pump power or output coupling. It is our hope to be able to investigate larger cavity transmissions (40-50%) in the near future. Figures 9 and 10 illustrate the variation of threshold pump power (P_{th}) and slope efficiency, respectively, with cavity output coupling for two lengths of fiber. Notice from Fig. 9 that, over the limited range in output coupling that has been investigated to date, P_{th} varies linearly with output coupling for both the 21 cm and 86 cm fibers. The slope efficiency data, however, give clear evidence for the onset of saturation.

The fact that the highest slope efficiency (> 24%) and output power are obtained from the short fiber is a direct consequence of ground state absorption. The green Ho^{3+} laser transitions terminate on various Stark sublevels of the ion ground state ($^5I_8$) and several experimental results clearly show the influence of re-absorption on the laser's performance. One area in which ground state absorption and depletion are manifested is the dependence of laser spectra on pump power that is illustrated in Fig. 11. Low resolution spectra recorded for three values of pump power (150, 185, and 240 mW) reveal a distinct shift to shorter wavelengths with increasing pump power which is attributed to partial depletion of the ground state population. Absorption measurements in the red ($^5F_5 \leftarrow {}^5I_8$ transition) confirm this result. For a fiber 21 cm in length, the absorption coefficient (α) at 643 nm, for example, declines by almost 50% (from its zero intensity value) as the pump power is increased to beyond 350 mW. For 250 mW of pump power, α has fallen from ~ 6% – cm^{-1} to 3.5% – cm^{-1}. Consequently, for the longer fibers studied in these experiments (80-90 cm), the available pump power is insufficient to significantly deplete the ground state and the laser behaves as a 3-level

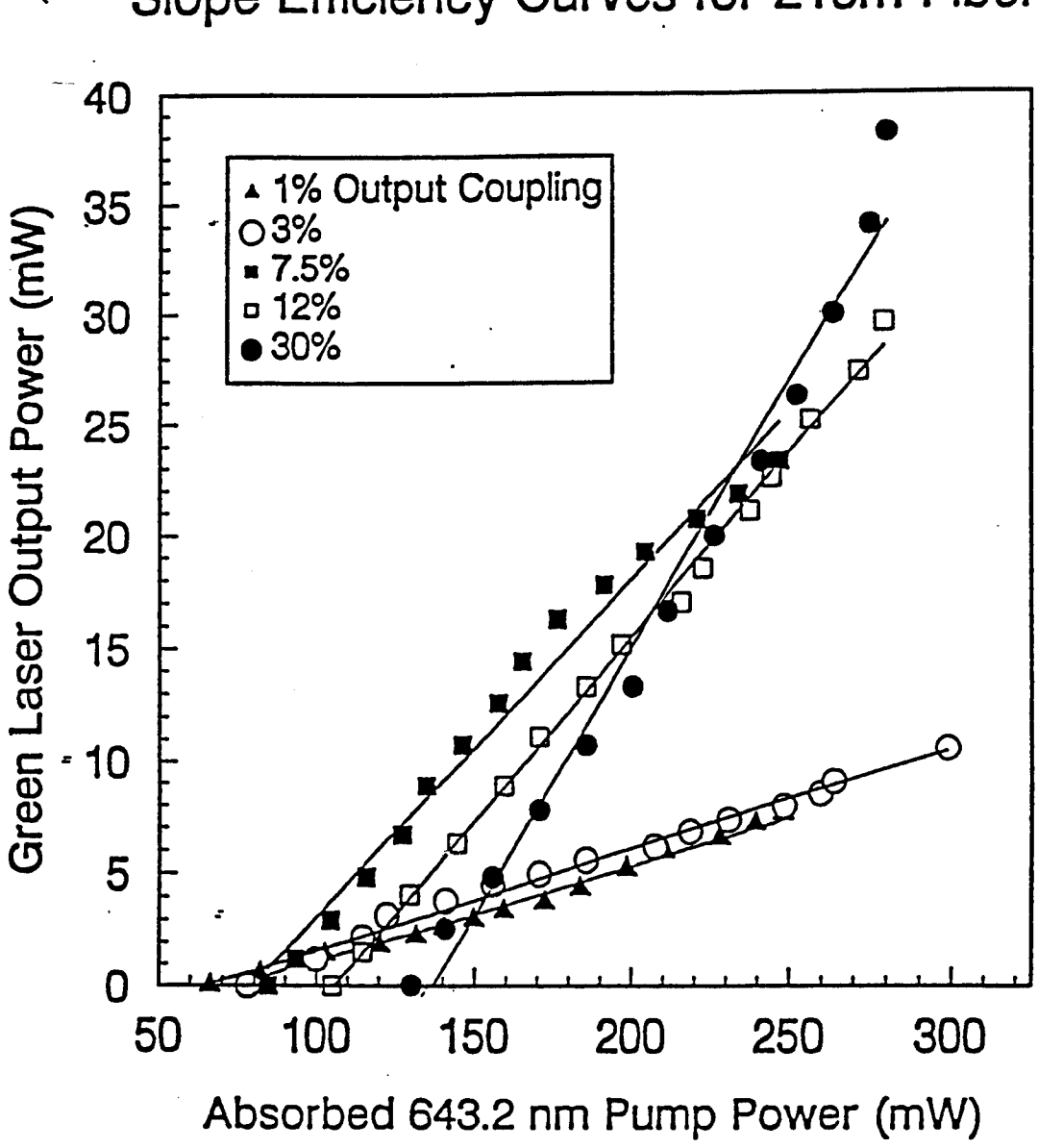

Threshold Power: 66 - 130 mW
Slope Efficiency: 4 - 24%
Max. Output Power: 38 mW

Figure 7 Dependence of Ho:ZBLAN fiber laser power on output coupling and pump power for a fiber 21 cm in length.

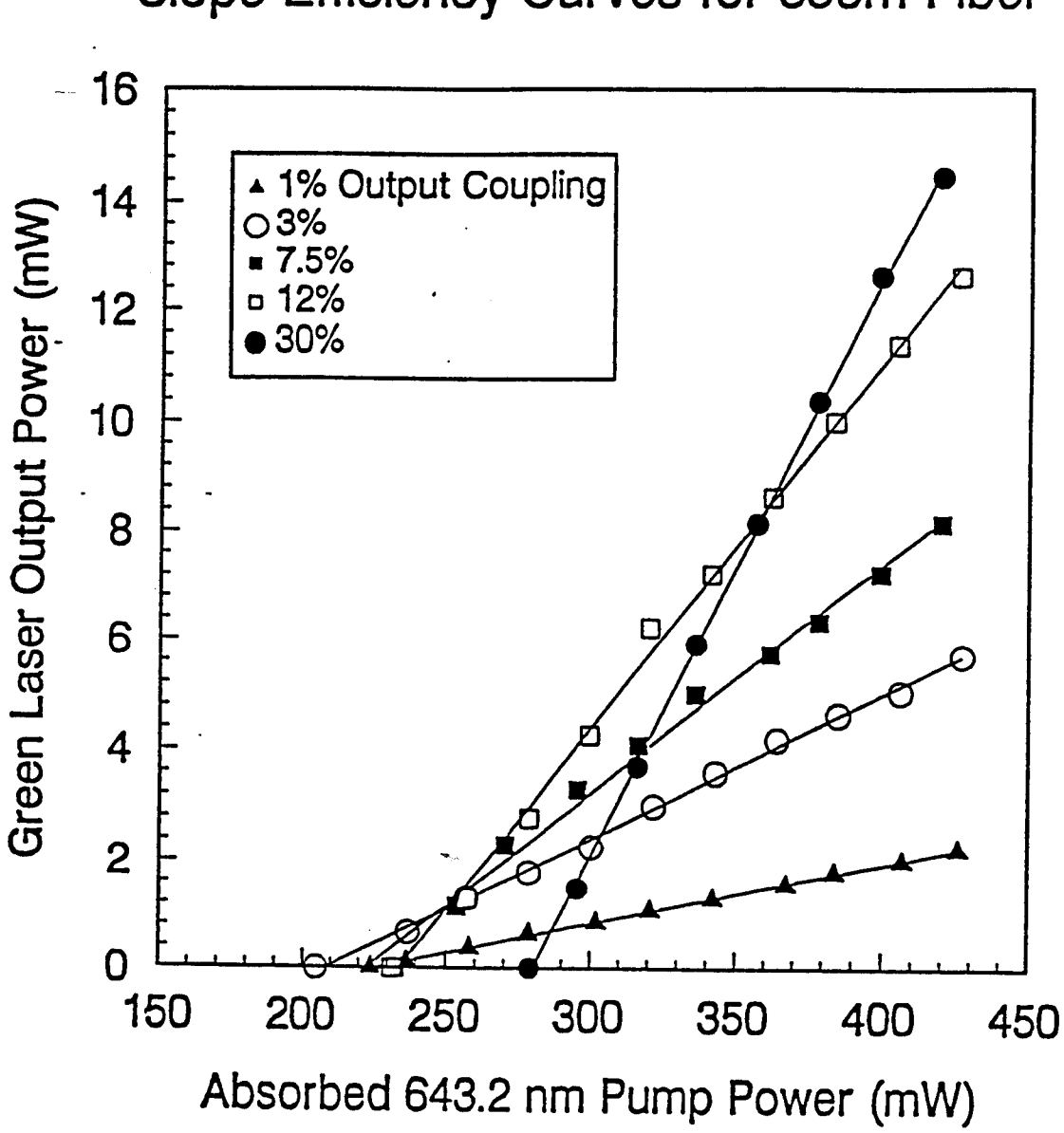

Threshold Power: 204 - 280 mW
Slope Efficiency: 1 - 10%
Max. Output Power: 15 mW

Figure 8 Data similar to those of Fig. 7 but for a fiber 86 cm in length.

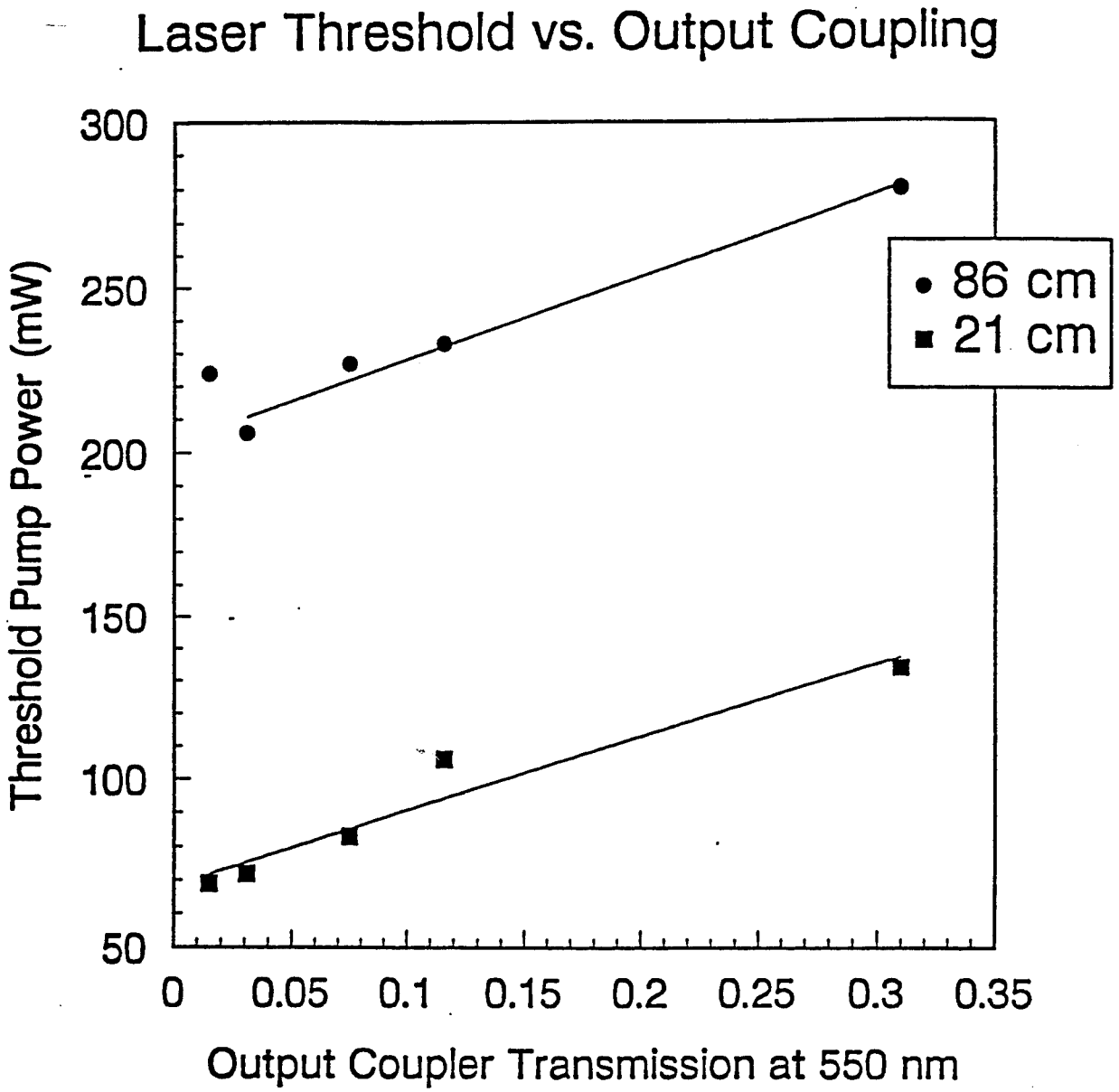

Figure 9 Variation of laser threshold pump power with cavity output coupling for the Ho:ZBLAN laser.

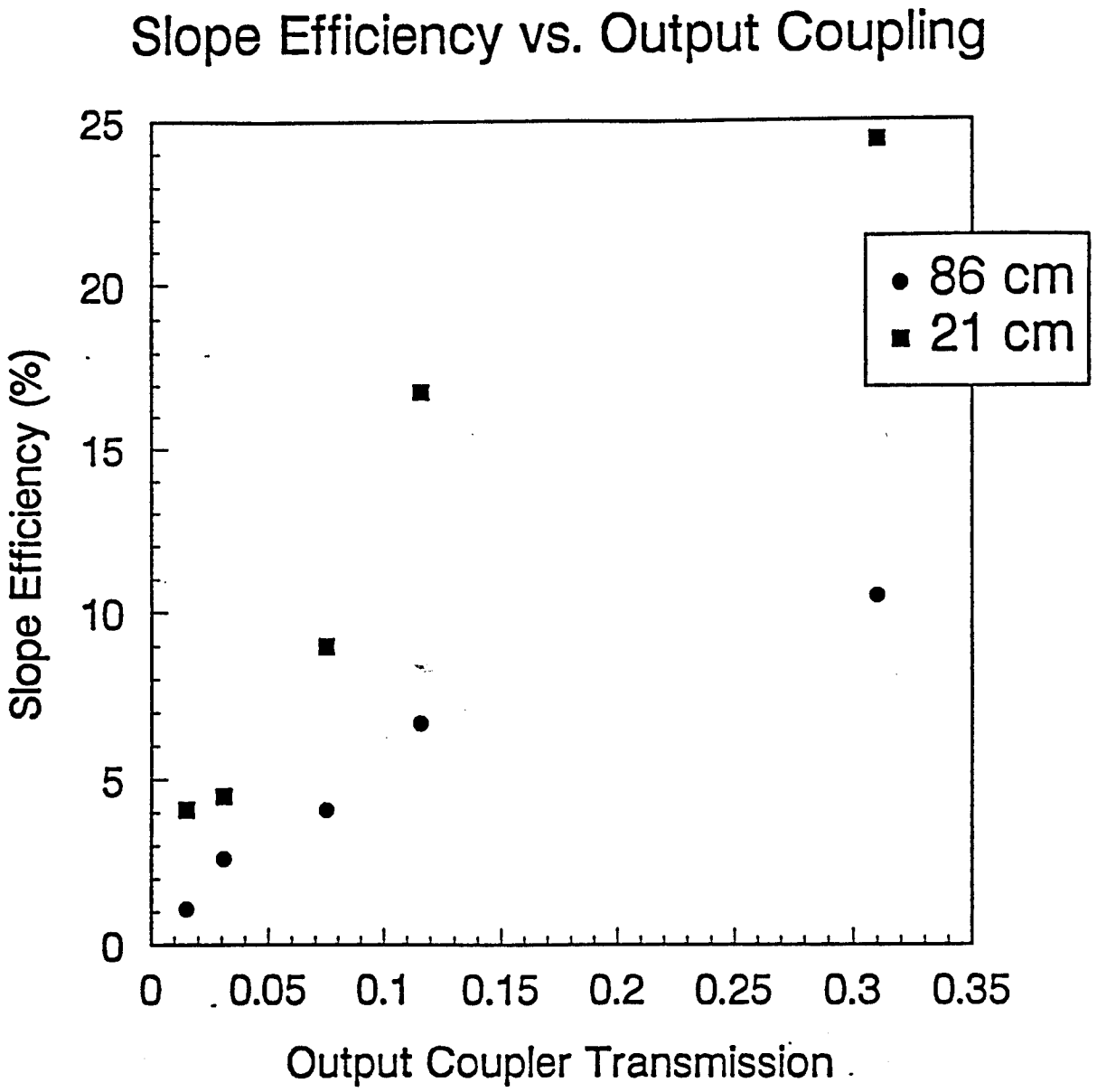

Figure 10 Dependence of slope efficiency on cavity output coupling for the Ho:ZBLAN laser.

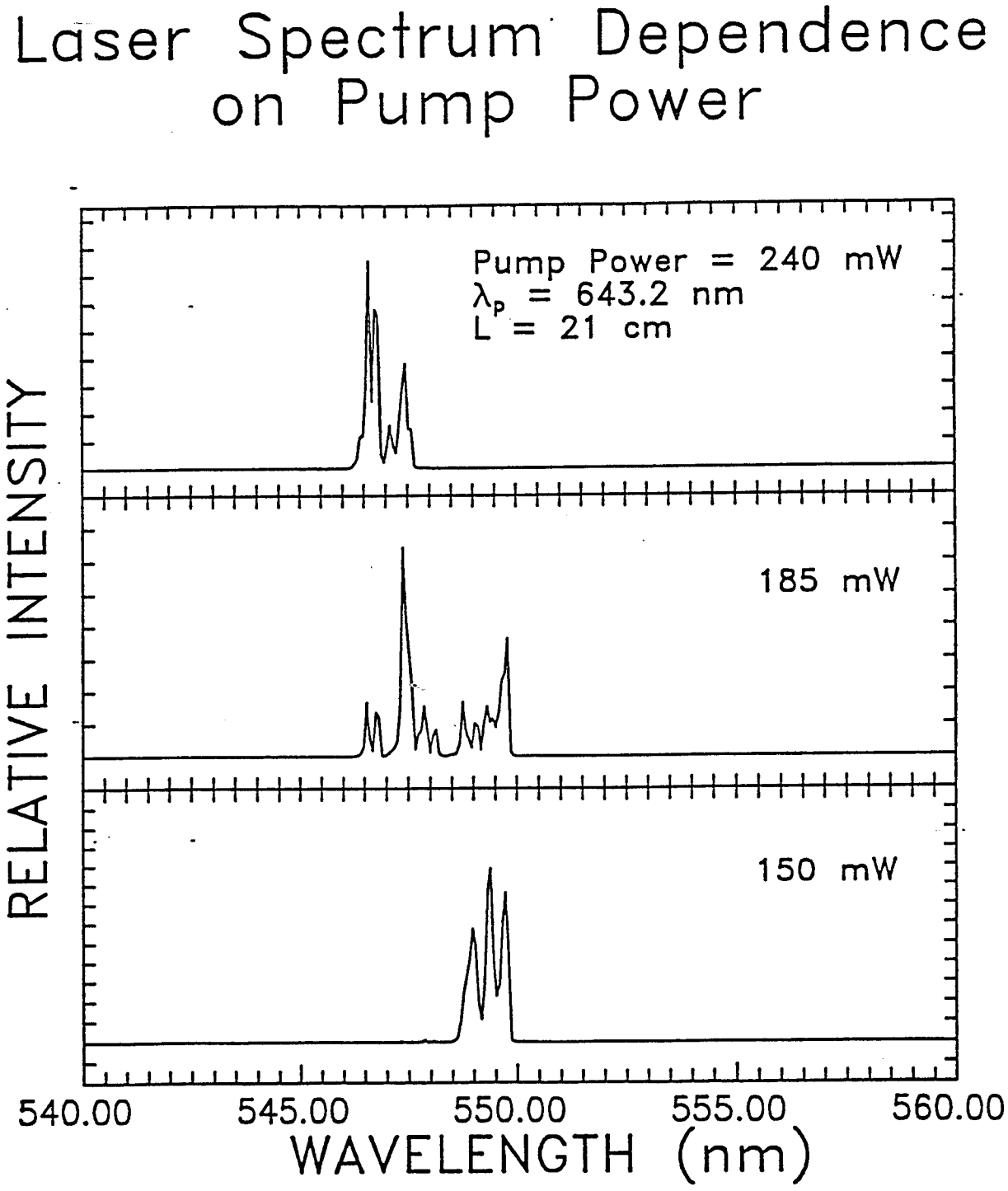

Figure 11 Ho:ZBLAN fiber laser spectra recorded at low resolution for different values of pump power.

system. In contrast, the 21 cm long laser is essentially a true 4-level system and is, understandably, considerably more efficient than its longer counterpart.

The performance of the laser at 77K also provides valuable insight into the nature of the lasing transitions. Figure 12 , for example, compares the room temperature and 77K laser spectra that were recorded for a fiber 19.5 cm in length that was pumped with 170 mW of 644 nm radiation. If we compare Figs. 11 and 12 (and similar data obtained at a variety of other pump power levels), it appears that cooling the fiber relaxes the upper state population, hence shifting the laser spectrum towards the red. Also, because cooling the fiber simplifies the laser spectrum considerably, we are in the process of analyzing the 77K spectrum of Fig. 12 in terms of the Stark level splitting in the upper laser level ($^5S_2$). Although the spectroscopy of rare earth ions in glasses is severely complicated (relative to crystalline hosts) because of the disordered nature of the glass and number of sites occupied by the ion, it does appear that analysis of the spectra from cooled fibers will permit us to elucidate the general characteristics of the emitting states.

Because of our interest in pumping this and similar systems with diode lasers, the excitation spectra (dependence of laser output power on pumping wavelength) were measured for the Ho:ZBLAN laser ($^5F_5 \leftarrow {}^5I_8$ transition) and the results are illustrated in Fig. 13 for several values of pump power. For most of the spectra shown, the power emitted by the 549.4 nm transition of Ho^{3+} was monitored as the excitation source was scanned in wavelength. Since the gain profile is inhomogeneously broadened and the Ho ions occupy at least two different sites in the glass, the spectra exhibit considerable structure and their widths increase with rising pump power. Note that because of the breadth of the excitation spectrum, diode laser pumping of this laser will not require the careful control over pump wavelength that is necessary with other diode-pumped solid state lasers. In summary, these results are quite intriguing and, in conjunction with modeling results to date, suggest that diode pumping of longer fibers (40-80 cm; optimal

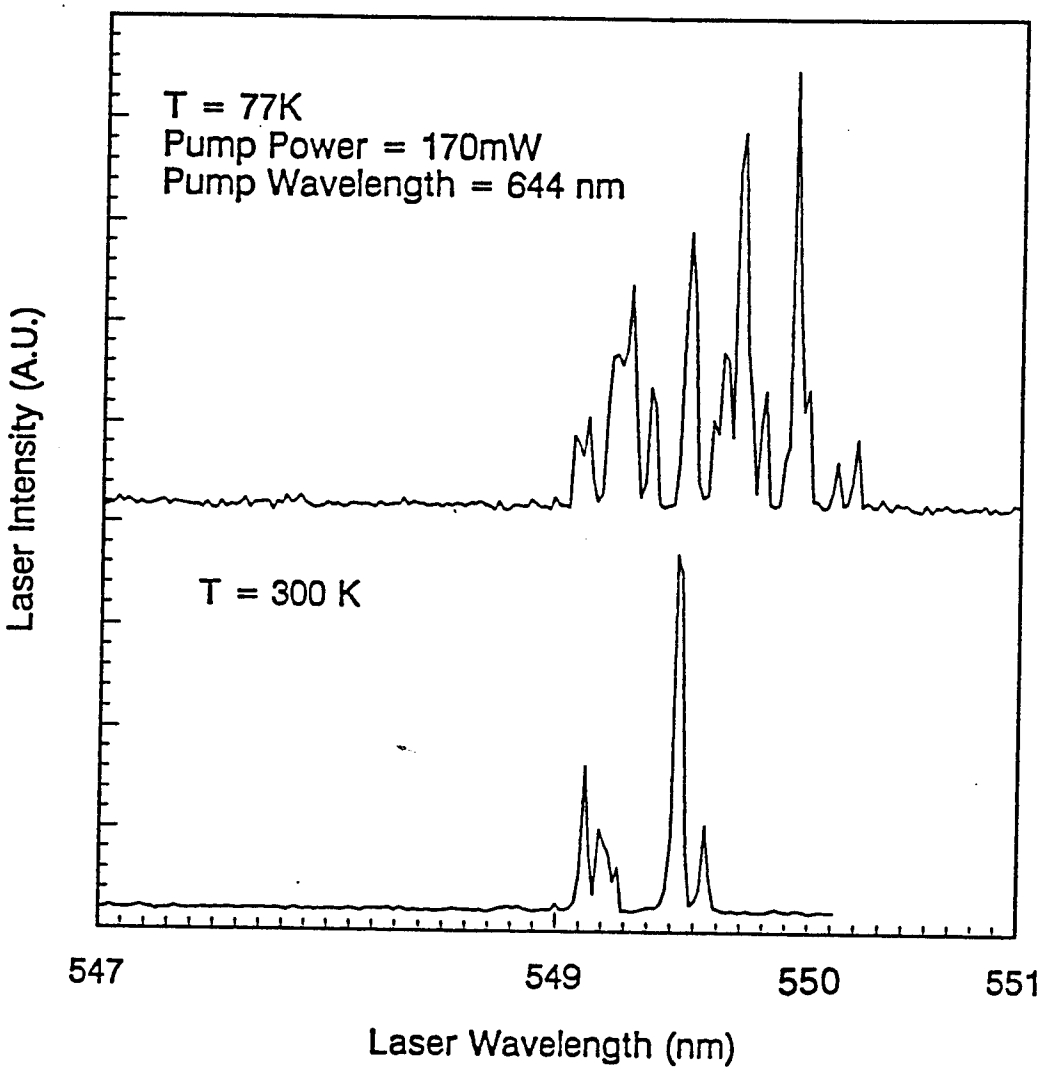

Figure 12 Comparison of room temperature and 77K spectra for the Ho:ZBLAN upconversion laser illustrating relaxation of the upper state Stark sub-levels. The complexity of the spectra results from the disordered nature of the host and the fact that at least two sites are occupied by the Ho^{3+} ion.

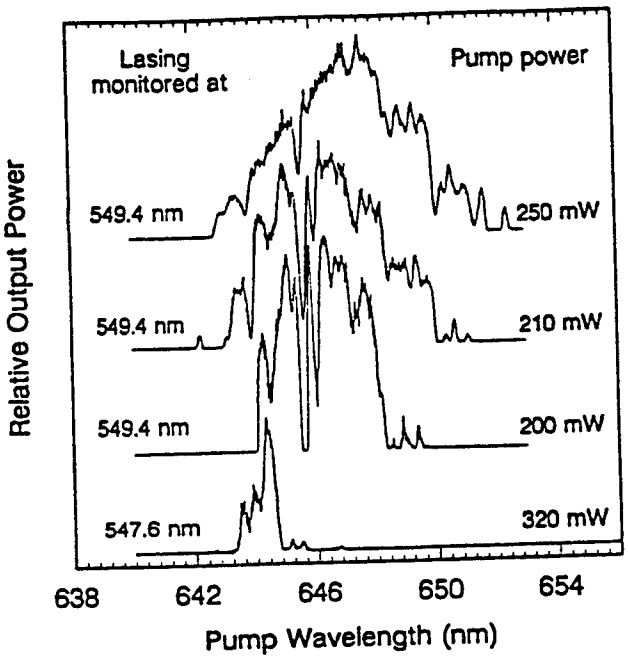

Figure 13 Excitation spectra for the Ho:ZBLAN fiber laser acquired by monitoring the output power of the indicated laser line as the pumping wavelength was scanned.

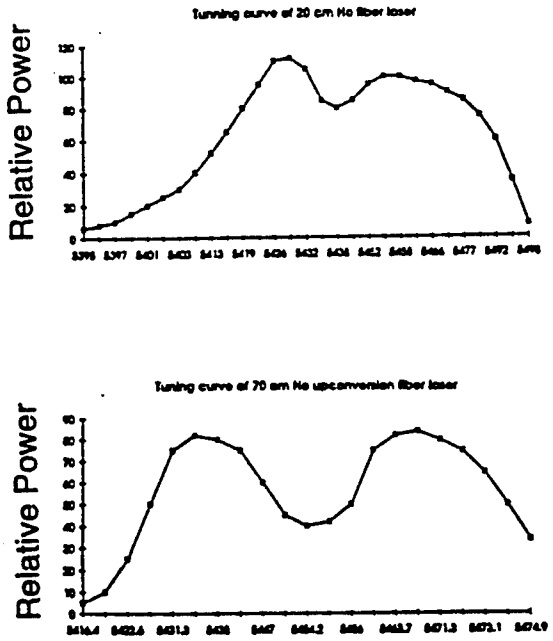

Figure 14 Tuning data for the Ho:ZBLAN laser using a multiple prism configuration.

length estimated to be 45 cm) should yield output powers in excess of 100 mW if sufficient pump power ($\geq$ 0.5 W) can be coupled into the fiber.

Before moving on to the next section, several other experiments should be mentioned briefly. One is that this laser has been tuned continuously with a cavity design in which the output coupling mirror is replaced by two mirrors (one spherical and one flat) and an etalon and/or several prisms. The tuning curves obtained at room temperature for both 20 and 70 cm long fibers are shown in Fig. 14. With careful adjustment, the laser will oscillate on a single transition of the "free-running" system. Secondly, the temporal behavior of the laser has been studied extensively. It exhibits, at higher pump powers, the spiking behavior observed from other fiber lasers. When the laser is driven at pump powers beyond ~ 250 mW, the output consists of bursts of pulses occurring at a PRF of 100 Hz. The individual pulses within the bursts have temporal widths of ~ 2 μs and the delay between pulses (inverse of the so-called "spiking frequency") decreases from ~ 12 μs at a pump power 1.6 times threshold to ~ 7 μsec at 2.6 times threshold. At lower pump powers, the laser acts as a true CW laser but, regardless of the pump power, the spatial profile of the output beam is excellent. We are also in the process of numerically modeling this laser and are attempting to mode-lock it with various solid state absorbers (including CdS particles in glass).

C. Fabrication of Planar Waveguides: Silver Diffusion, Laser Ablation

Eventually, integrating rare earth-based upconversion lasers with modulators, diode lasers and passive waveguides will require that techniques for fabricating planar waveguides of rare earth-doped glasses be developed. Over the past several years, considerable effort has been devoted to developing rare earth lasers in planar waveguides in which the host is a crystal or silica glass and Table I summarizes the properties of several of these. Note, however, that all of the systems demonstrated to date lase in the IR or near-IR largely because the phonon spectra of the hosts investigated to date are

Table 1. Examples of solid-state lasers in waveguides and bulk materials that have been demonstrated to date.

Ion:Host, type	Pump Wavelength(s) (nm)	Laser Wavelength(s) (nm)
Nd:$LiNbO_3$, guide Er:$LiNbO_3$, guide	814 1479	1085 1576
Nd:$LiTaO_3$, guide	750	1092, 1076
Yb:YAG, bulk	940	970,1030
Nd:YAG, guide	590, 800	1064
Nd:phosphate glass, guide	790	906, 1057, 1358

unfavorable to upconversion (or sequential absorption of two or more photons) pumping of more highly-excited states.

For these reasons, we are interested in fabricating planar waveguides of rare earth-doped, heavy metal glasses, with emphasis on the fluorides. Two approaches are presently being pursued: in-diffusion of Ag or possibly Au (or, for crystalline, waveguides, Ti) in bulk glass or deposition of thin, rare earth-doped glass films.

Although Ag-diffused waveguides in silica glasses are quite common, comparatively little is known of processing the fluoride glasses and how one might fabricate single mode waveguides, in particular. Furthermore, silica glass waveguides can be fabricated by Ag-Na exchange in molten salt baths but this is not viable with fluoride glass. The latter requires careful handling since it is brittle and susceptible to thermally-induced fracture. After considerable experimentation, we have demonstrated a two-step technique whereby Ag can be driven into the bulk glass under the influence of an electric field, forming layers that are more than 2.5 μm in thickness. The technique involves depositing silver and aluminum electrodes on a polished sample, heating the glass to ~ 250°C and diffusing the silver (under vacuum) with an electric field of typically 30 $V - cm^{-1}$. Secondary ion mass spectrometry (SIMS) analysis of the samples

such as that shown in Fig. 15 verify the diffusion into the bulk and suggest that Na in the ZBLAN host is, indeed, being displaced. We are, in collaboration with a group at NIST in Boulder, CO, currently testing these structures as planar waveguides and future work will investigate the use of other Group IB atoms such as Cu and Au.

A second approach to fabricating planar waveguides is to produce thin films by physical or chemical processes. Because of the complex stoichiometry of the fluorozirconate glasses, our initial work has focused on the latter and we have deposited Ho:ZBLAN films on a variety of substrates by laser ablative deposition. An ArF laser (193 nm) provided the optical beam and the substrate temperature was typically beyond 200°C. Films several microns thick can be readily deposited in this way and measurements of scattering losses are underway. The first experiments (carried out in vacuum) produced particulates $\lesssim 3$ μm in diameter in the films that adversely affect their optical quality. We are in the process of introducing a rare gas to the reactor and reorienting the substrate to suppress particle formation and we are convinced that this approach will yield films of more than adequate optical quality.

D. Development of a Molecular Anti-Stokes Raman Laser: Observation of Gain in the Deep UV

We have recently observed gain in the deep UV ($\lambda \sim 225$ nm) on the $G \rightarrow X$ (bound-free) transition of Hg_2. The significance of this result is that gain was produced, not in the usual manner, but by a stimulated electronic Raman scattering process in which the metastable $A\,O_g^+$ state of Hg_2 served as the storage (initial) level. In other words, this result is the first step towards realizing an anti-Stokes Raman laser (ASRL) in a molecule. Although the work to be described here does not constitute a major fraction of this AFOSR program (only one graduate student is involved), it represents the culmination of several years of work and the potential "payoff" is large. For several years now, our laboratory has been developing and applying spectroscopic techniques for examining Rydberg states of small molecules having dissociative ground states. Without detailed

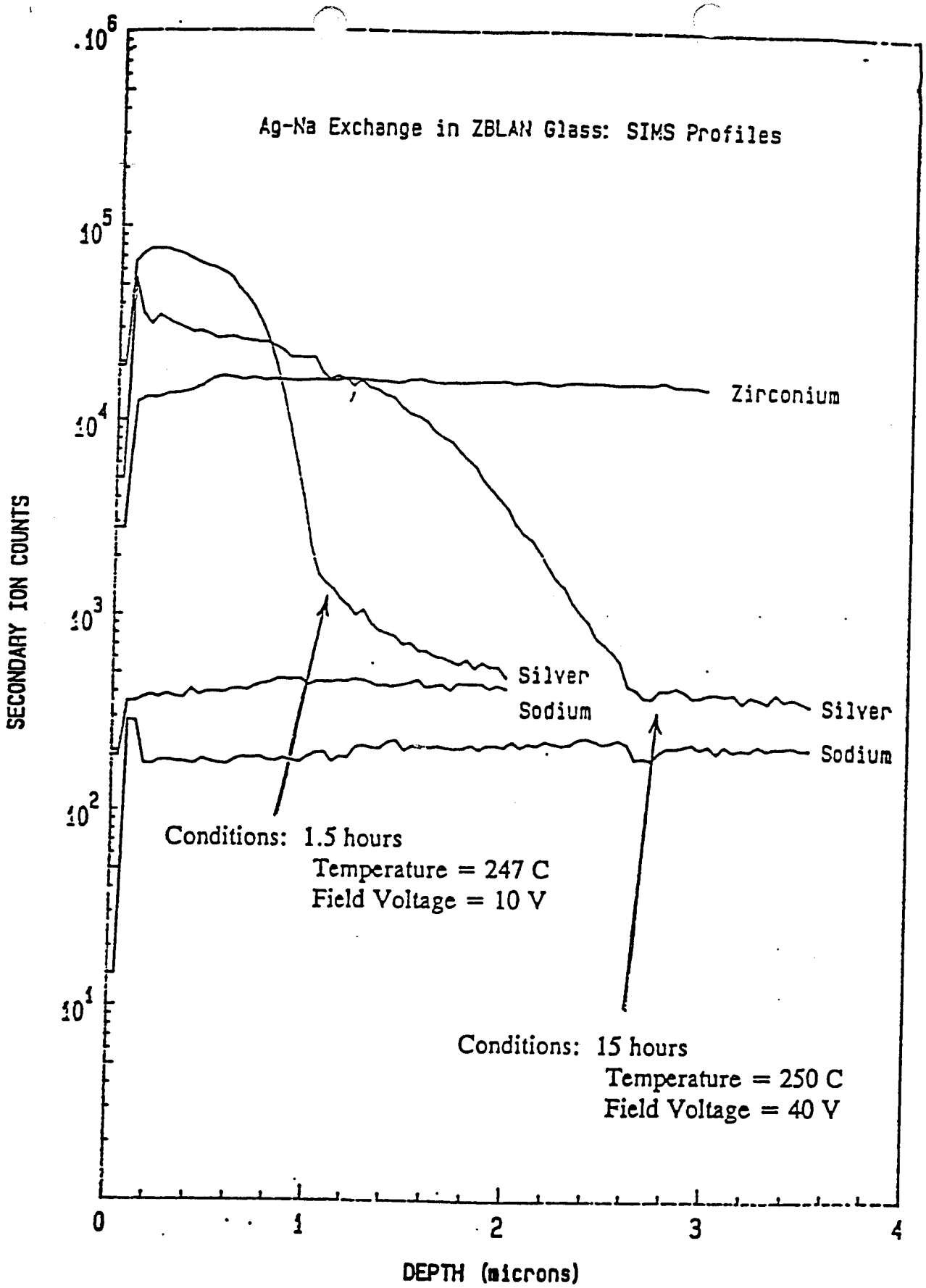

Figure 15 SIMS depth profiles for silver diffused into ZBLAN. The results for two samples are shown and the processing conditions for each case are indicated.

spectroscopic information concerning the structure of such molecules, designing an ASRL is impossible. As discussed in this section, sufficient information is now available and our experimental results strongly suggest that a practical system is now within reach.

It has long been known that energy can be efficiently stored in the lowest excited states of the Group IIB dimers. The predecessor of DOE (ERDA) supported work to investigate the excimer transitions of Hg_2 and Cd_2 (470 nm), in particular, as potential energy storage lasers in the mid-1970s but the stimulated emission cross-section proved to be too small and excited state absorption appeared to be responsible for the observation of net loss. Therefore, the conventional approach of requiring the upper laser to have a reasonable stimulated emission cross-section and, at the same time, be capable of efficiently storaging energy imposes a strict requirement that has proven difficult to meet. The ASRL approach effectively decouples these two issues and is likely to yield sources of greatly improved characteristics.

Figure 16 shows lifetime data for the $A\,O_g^+$ state of Hg_2 that was obtained by a pump-probe experiment in our laboratory. The O_g^+ level was populated indirectly by Hg-Hg photoassociation at 266 nm to produce the 1_u state which subsequently was quenched by collisions to the O_g^+ level. A time-delayed, laser-induced fluorescence probe pulse permitted the temporal history of the $A\,O_g^+$ relative number density to be measured. At low Hg vapor pressures, the decay of the A state population is best described by a double exponential owing to the presence of nearby states (and 1_u, in particular). The relevant point to be made from these data is that, even for Hg vapor pressures of several Torr, the effective lifetime for the $A\,O_g^+$ state is > 1 μsec.

Furthermore, Hg_2, Cd_2 and Zn_2 excited states lying as high as ~ 7 eV in energy have recently been observed and characterized by laser spectroscopy. Of particular interest are the $^1\Sigma_u^+$ (O_u^+) levels that are derived from the $^1P_1$ resonance state and a ground state atom. These states satisfy all of the criteria that one requires of an intermediate state in an anti-Stokes Raman scheme. Specifically: 1) they are optically

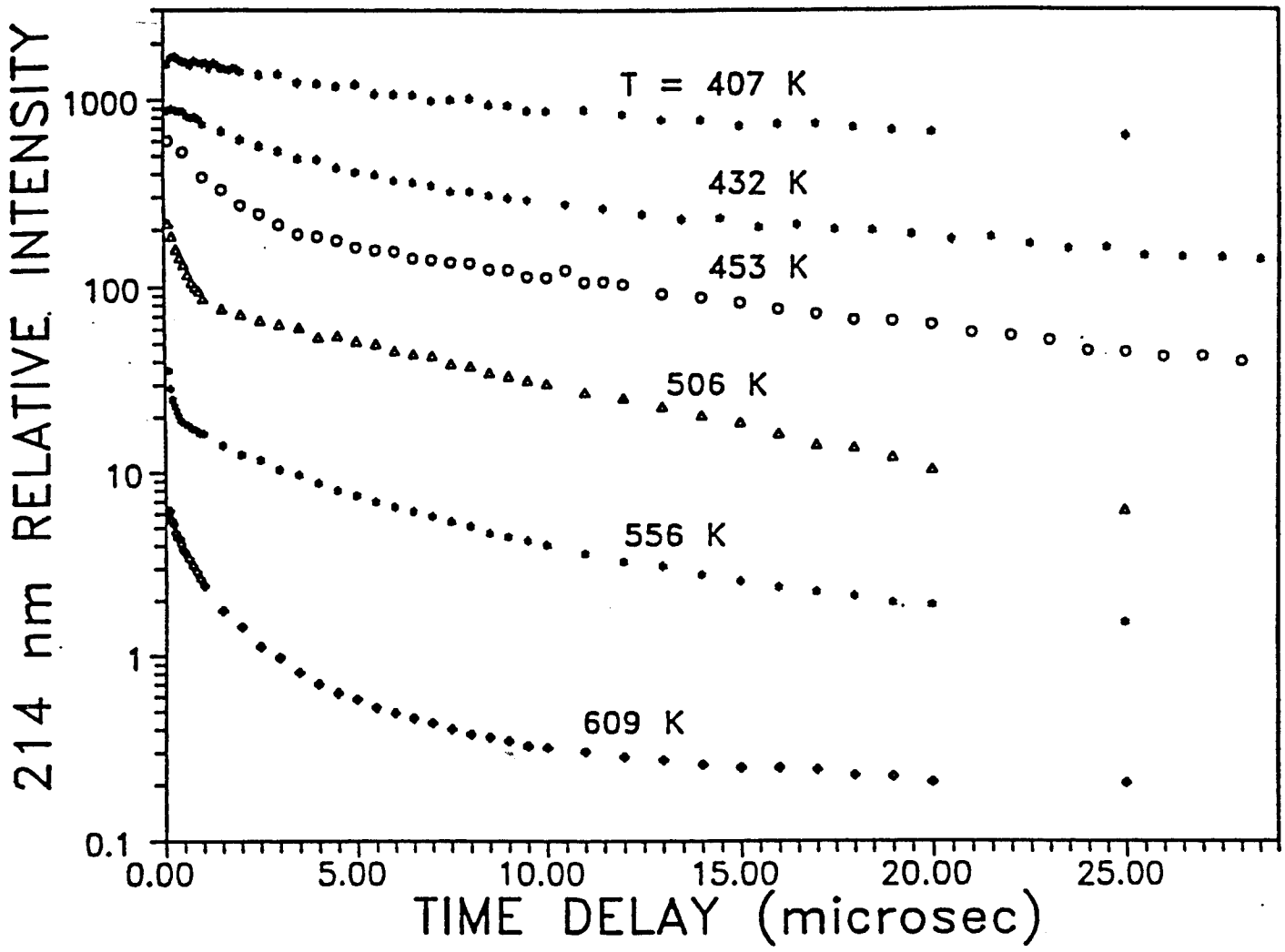

Figure 16 Temporal variation of the Hg_2 AO^+_g state population measured by a laser pump-probe technique in our laboratory. The curves for the various temperatures (Hg vapor pressures) have been intentionally offset from one another for the sake of clarity. Consequently, it is not possible to compare relative intensities between the sets of data.

connected to both the storage ($A\,O_g^+$) and ground ($X\,O_g^+$) states by single photon transitions (the lowest $^1\Sigma_u^+$ (O_u^+) states in Hg_2, Cd_2, and Zn_2, for example, have radiative lifetimes < 5 ns), 2) the electronic moments for both the $O_u^+(I) \leftarrow O_g^+(S)$ and $O_u^+(S) \rightarrow O_g^+(T)$ transitions are estimated to be large (≥ 1 D), and 3) the branching ratios for emission from the intermediate O_u^+ state favor transitions to ground. Emission experiments conducted in this laboratory and elsewhere have characterized these states in some detail. The $G\,O_u^+$ ($^1\Sigma_u^+$) states of Zn_2 and Cd_2 have been observed in emission in our laboratory and Fig. 17 shows the characteristic undulatory emission spectrum (known as Condon internal diffraction) that is observed from the $v' = 85$ level of Zn_2 when the $^1\Sigma_u^+$ excited state is produced directly by the photoassociation of Zn-Zn atomic pairs at 222 nm. Similarly, the fluorescence spectra of Fig. 18 are the result of emission form the $v' = 9$ or $v' = 1$ states of Hg_2 ($G\,O_u^+$) that were populated by pumping the (9,0) and (1,0) transitions of the G ← A transition at 564.7 or ~ 614 nm, respectively. Note that the "diffraction" patterns indicate that the emission is emanating almost solely from $v' = 9$ or $v' = 1$ (depending on the pump wavelength). In summary, the approach to a molecular ASRL being pursued in this program exploits: 1) the metastability of $O_g^\pm$ in Hg_2 and Cd_2 ($^{1,3}\Pi_g$ in Zn_2), and 2) recent spectroscopy of more highly excited states in these molecules that has now made it possible to choose an intermediate state having the proper characteristics. Note that the $A\,O_g^+ \rightarrow G\,O_u^+ \rightarrow X\,O_g^+$ anti-Stokes scheme in Hg_2 would give a Stokes shift of > 3.5 eV – that is, a yellow photon generates a deep UV (~225 nm) photon. The use of higher-lying O_u^+ states as intermediate levels would make it possible to move into the VUV. Furthermore, it is clear from Fig. 18 that another feature of this approach is the ability to "synthesize" a gain spectrum by resorting to two or more pumping (G ← A) wavelengths. The composite spectrum will be a linear combination of the individual gain spectra. It should also be emphasized that Hg_2 was chosen for initial studies because its excited state structure is sufficiently well known that worthwhile calculations can be made. Other systems, such as OH, are also attractive.

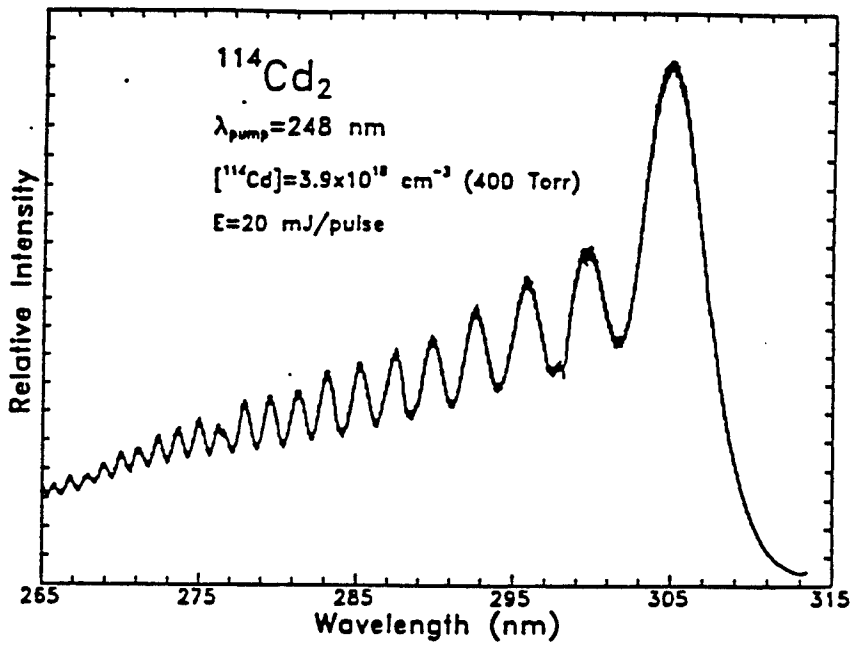

Figure 17 Emission spectrum (known as Condon Internal Diffraction) for the $v' = 58$ level of the O_u^+ state of Cd_2 correlated with $5p^1P_1 + {}^1S_o$.

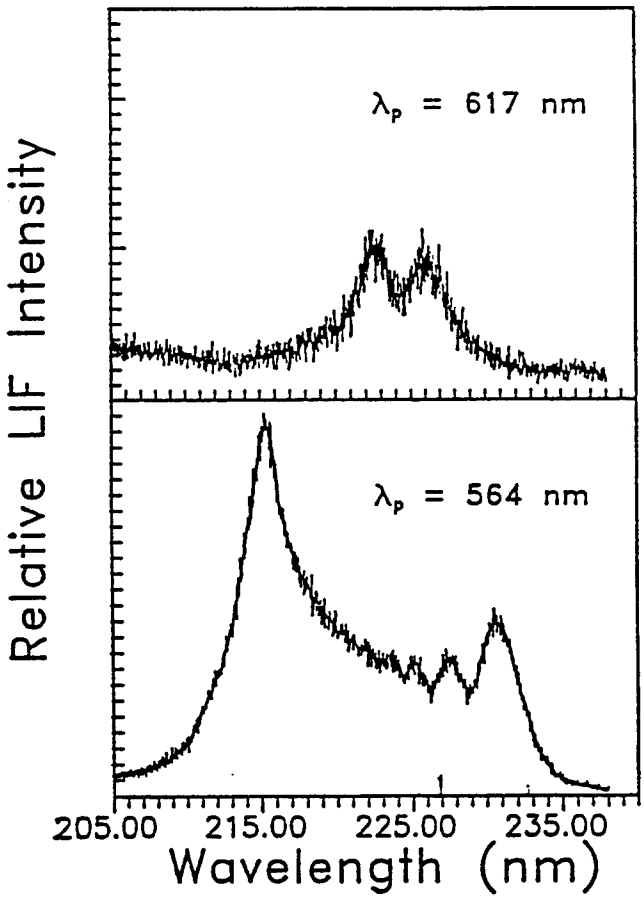

Figure 18 Spectrum similar to that of Fig. 17 but for the $v' = 9$ and $v' = 1$ levels of the GO_u^+ state of Hg_2. In this instance, the emitting state was populated by a pulsed dye laser tuned to the (9,0) or (1,0) transition of the $GO_u^+ \leftarrow AO_g^+$ band. Although somewhat noisy (because no effort has yet been made to average the spectra from several shots), the correct number of oscillations expected for both reflection spectra are observed.

Observation of Gain: Hg_2 (G → X) Transition

Experiments to determine the feasibility of producing gain on the G → X transition of Hg_2 via the $A\,O_g^+ \rightarrow G\,O_u^+ \rightarrow X\,O_g^+$ scheme anti-Stokes Raman scheme described above and shown schematically in Fig. 19(a) were conducted with the arrangement of Fig. 19(b). For convenience, Hg_2 molecules in the A state were produced indirectly by photoassociating Hg-Hg collisions pairs at 266 nm to access the 1_u state (lying ~ 2000 cm^{-1} above the $O_g^{\pm}\ 1_g$ group of states). Collisions with background atoms subsequently de-activate 1_u and populate the A state. An adjustable time delay later (typically 0.2 μs), a dye laser having a linewidth of ~ 0.2 cm^{-1} drives the (9,0) band of the G ← A transition and the presence or absence of gain in the deep-UV (G → X transition) is detected with the frequency-doubled output pulse of a second dye laser (operating at nominally 450 nm). Initial experiments were conducted by tuning the probe dye laser to ~ 227 nm which coincides with the longest wavelength undulation in the $v' = 9$ emission spectrum (cf. Fig. 18). Repeated measurements demonstrate that gain is, indeed, present. As illustrated by the superimposed gain waveforms of Fig. 20, peak gain of almost 0.6% - cm^{-1} is measured at 227.5 nm when the G ← A transition is pumped at 564.73 nm ((9,0) band). For these experiments, the Hg number density, [Hg], is 7.1 x 10^{18} cm^{-3} and the 266 nm pulse energy was 4 mJ. Under these conditions, the peak $Hg_2(A)$ population is estimated to be $5 \cdot 10^{14}$ cm^{-3} (assuming the reduced Hg-Hg photoassociation cross-section at 266 nm to be the same as the 193 nm value – 10^{-38} cm^5). If, therefore, we estimate the other relevant constants in eqn. (1) to be $\lambda_p = 0.56$ μm, $\lambda_{AS} = 227$ nm, $|eR_{GX}|^2 \approx (2D)^2$, $|eR_{AG}|^2 \sim (1D)^2$, N_T ([Hg(X)]) ≈ 0, $q_{AG} = 0.086$, $q_{GX} \approx 5 \cdot 10^{-2}$ $h\Delta\omega_{AG} = 0.5\ cm^{-1}$ and $h\gamma = 0.2\ cm^{-1}$, then

$$\alpha \approx 6.7 \cdot 10^{-24}[Hg_2\,(A\,O_g^+)]\ I_p\ (cm^{-1}) \qquad (1)$$

or

$$\alpha \approx 2.7\ \%\ -\ cm^{-1}$$

(a)

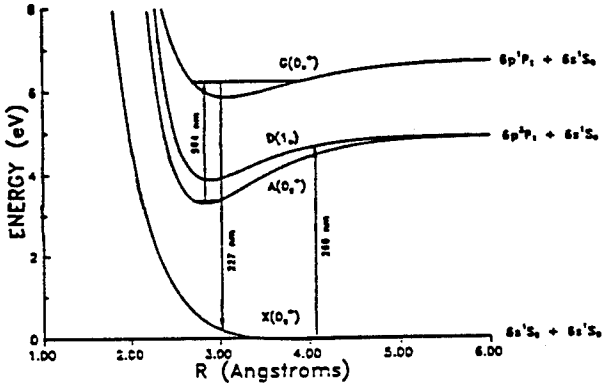

(b)

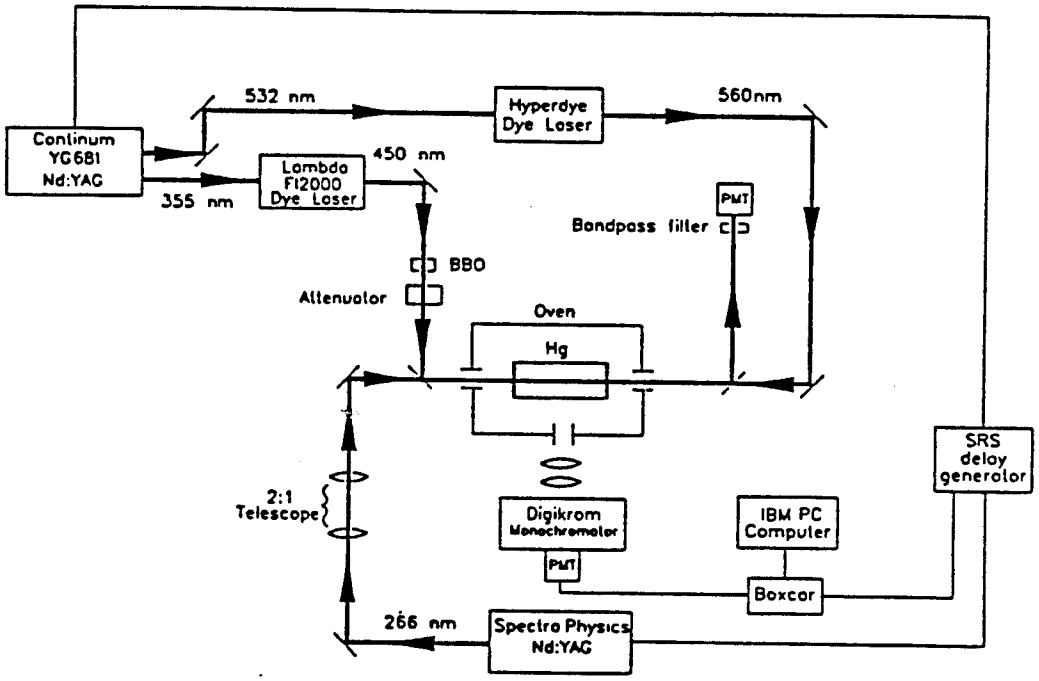

Figure 19 (a) Partial energy level diagram for Hg_2 illustrating the storage of energy in the $A\,O_g^+$ metastable state and the extraction of deep UV radiation by the electronic anti-Stokes Raman process; (b) Schematic diagram of the experimental apparatus for the measurement of gain on the G → X transition of Hg_2. $A\,O_g^+$ metastables are produced by photoassociation of Hg-Hg pairs at 266 nm to form 1_u molecules; subsequent collisional quenching of the 1_u state populates the $A\,O_g^+$ level.

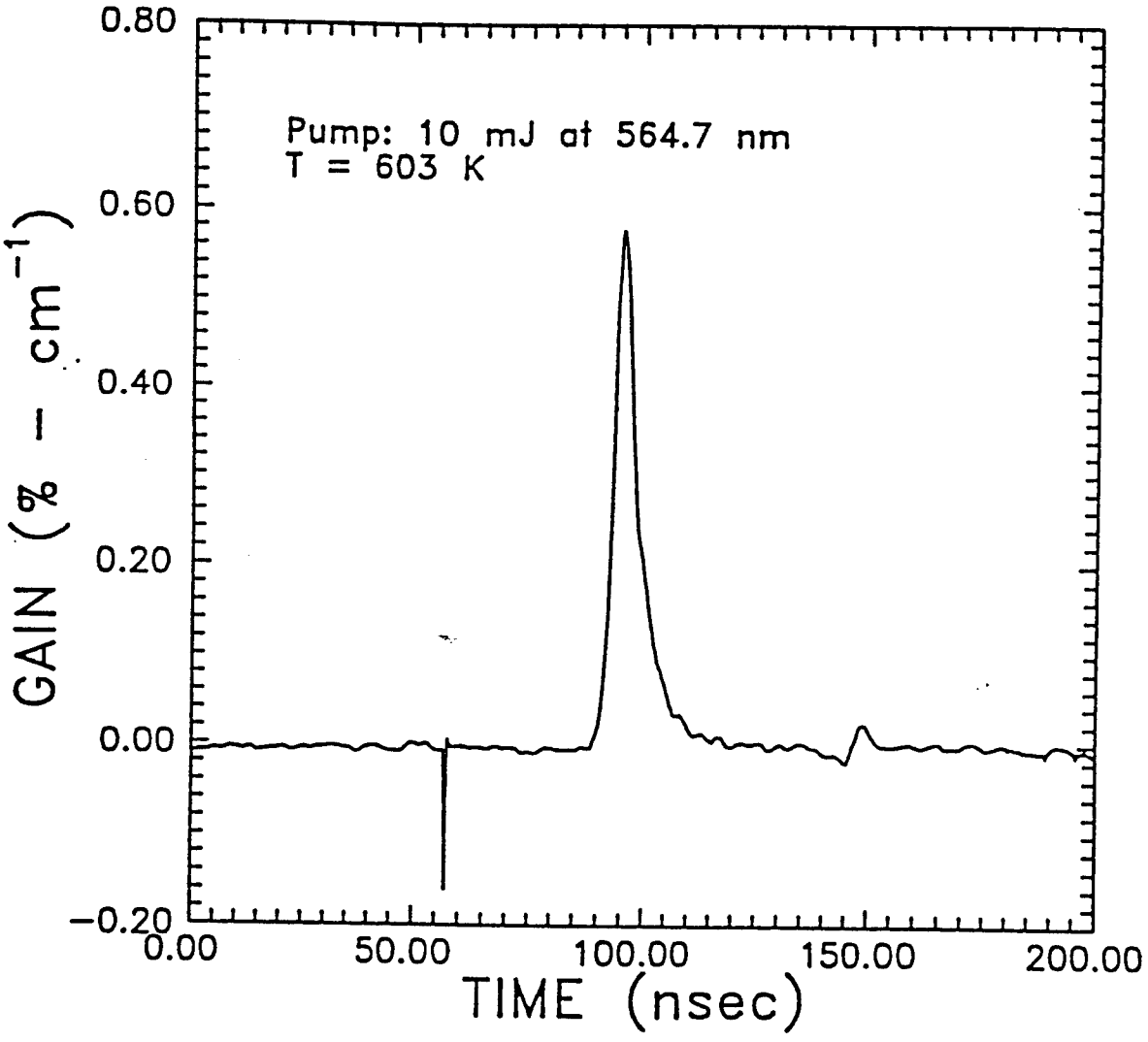

Figure 20 Measurement of gain on the G → X band of Hg_2 at 227.5 nm—the peak gain coefficient observed is ~ 0.6% – cm^{-1}. The waveform shown is actually 100 superimposed pulses which illustrates the reproducibility of the results. The spike at 60 ns is an artifact of the experiment but serves as a convenient fiducial mark.

for $[Hg_2] \approx 5 \cdot 10^{14}\ cm^{-3}$ and $I_p = 8.0\ MW - cm^{-2}$.

This calculation takes into account the fact that, at 300 K, the Hg_2 (A, v = 0) rotational level having the largest population at thermal equilibrium is

$$J_{max} = \left(\frac{kT}{B_v}\right)^{1/2} = 70 \qquad (2)$$

where B_v is the effective rotational constant for the $Hg_2(A)$ state ($0.021\ cm^{-1}$) and the fraction of the $A\,O_g^+$ population residing in that one level is ~ 0.9%—i.e., $[Hg_2(A\,O_g^+)]_{v=0,J_{max}} = 9 \cdot 10^{-3}\ [Hg_2(A)]$. Also note that the laser detuning chosen here ($h\Delta\omega_{AG} = 0.5\ cm^{-1}$) is large compared to the molecule's rotational constant. Consequently, it should be possible to tune this ASRL nearly continuously over hundreds of cm^{-1} in the deep UV. In more recent experiments, gain has been observed over a ~700 cm^{-1} region around 230 nm. This result is consistent with the spectrum of Fig. 18 (bottom) and gain probing measurements at shorter wavelengths are in process.

We conclude that the experimentally observed gain coefficient is *consistent* with crude calculations. (Accurately estimating the A state population is problematic because of the other electronic states lying in the vicinity.) Despite this result, it must be emphasized that because the resolution of the experiments carried out to date is not sufficient to resolve individual rotational lines, it is not possible in high pressure background ("bulb") experiments (apparatus of Fig. 19(b)) to positively demonstrate the de-tuning behavior that is a signature of an ASRL system. Nevertheless, these results demonstrate that a population inversion between the A and X states of the dimer has been established and that realizing an ASRL is within reach.

E. Generation of Coherent UV Emission by Parametric Processes in Metal Vapors with Femtosecond Pulses

In recent experiments, the conversion of red femtosecond laser pulses into the UV by a four wave parametric process has been demonstrated. Our motivation in conducting these studies is the desire to efficiently convert subpicosecond pulses from the visible or near-IR to the ultraviolet with efficiencies exceeding those obtainable by SHG or continuum generation.

The generation of coherent UV by parametric processes in the alkali metal vapors has been known for two decades. All prior experiments, however, have been conducted on the nanosecond time scale and involved a two color pumping scheme. The experiments carried out in our laboratory were based on the 4 wave parametric process: $2\omega_1 - \omega_2$ in which the pumping photons were supplied by a pulse-amplified CPM laser system producing ~ 1/3 mJ, 80-120 fs pulses. A partial energy level diagram for atomic potassium, illustrating the states involved in the parametric process, is given in Fig. 21. The red (λ ~ 625 nm) output of our amplified CPM system overlaps the two photon $8^2S_{1/2} \leftarrow\leftarrow 4^2S_{1/2}$ transition of K and the intensity of the pump (weak focus; I_m ~ 4 GW – cm^{-2}) is sufficient to induce hyper-Raman scattering on one of several IR transitions and parametric oscillation in the UV. Figure 22 presents the dependence of the UV output energy on the femtosecond pulse energy and shows clearly that the onset of emission has a well-defined threshold.

The strongest observed lines are the $7p\ ^2P_{1/2,3/2} \rightarrow 4s\ ^2S_{1/2}$ and $6p\ ^2P_{1/2,3/2} \rightarrow 4s\ ^2S_{1/2}$ transitions that lie at 321 and 344 nm, respectively, and beam cross-sectional intensity measurements at each of these wavelengths (and others, such as 404 nm) show the spatial coherence of the emitted radiation to be high. Although we have not autocorrelated the UV pulses to determine their precise temporal widths, measurements made with pin photodiodes demonstrate that they are certainly < 50 ps in duration.

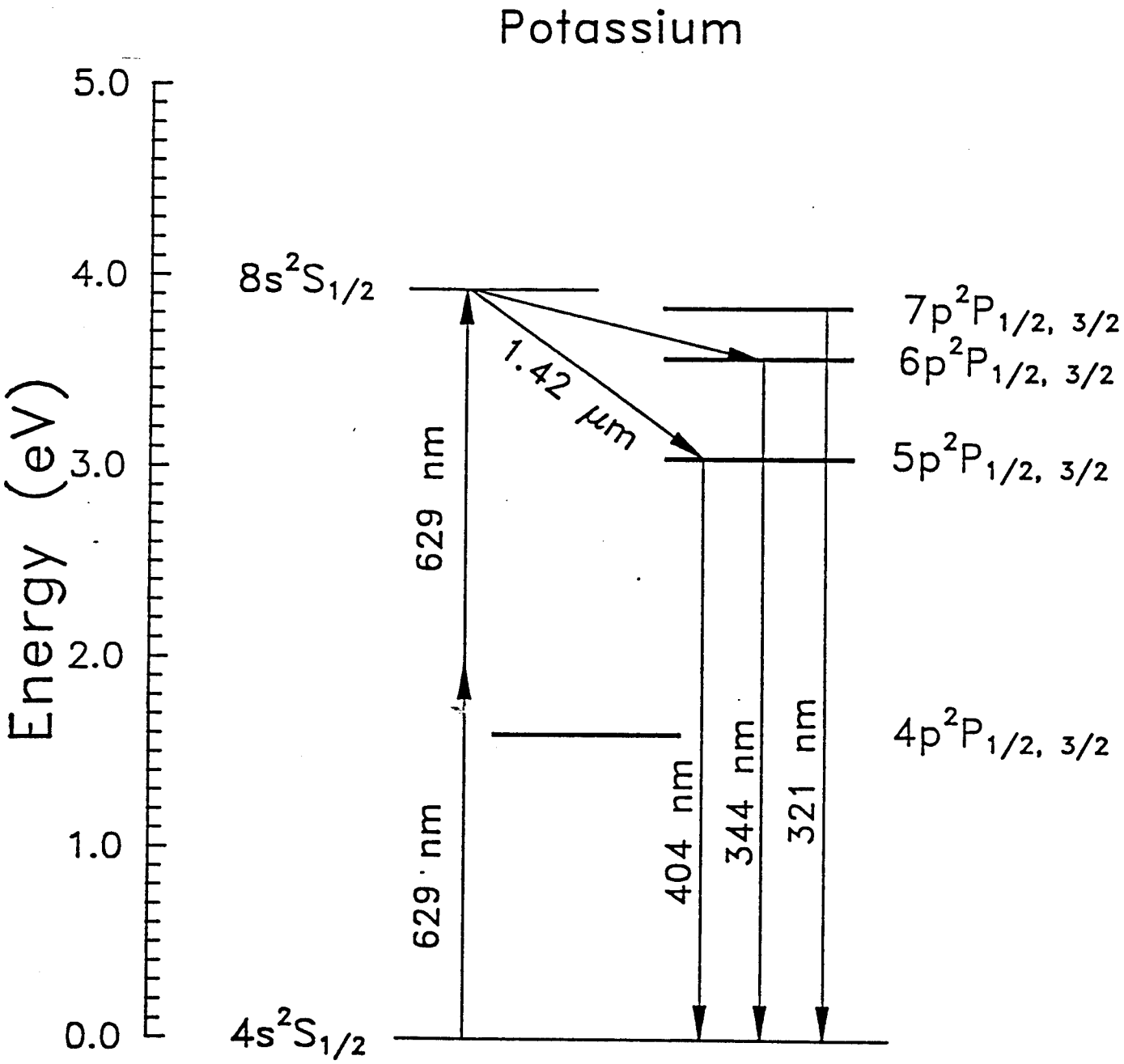

Figure 21 Partial energy level diagram for atomic potassium showing the process by which coherent UV is produced from red femtosecond pulses. Similar results are obtained with rubidium although the resulting UV wavelengths are somewhat shorter ($\lambda \simeq 300$ nm).

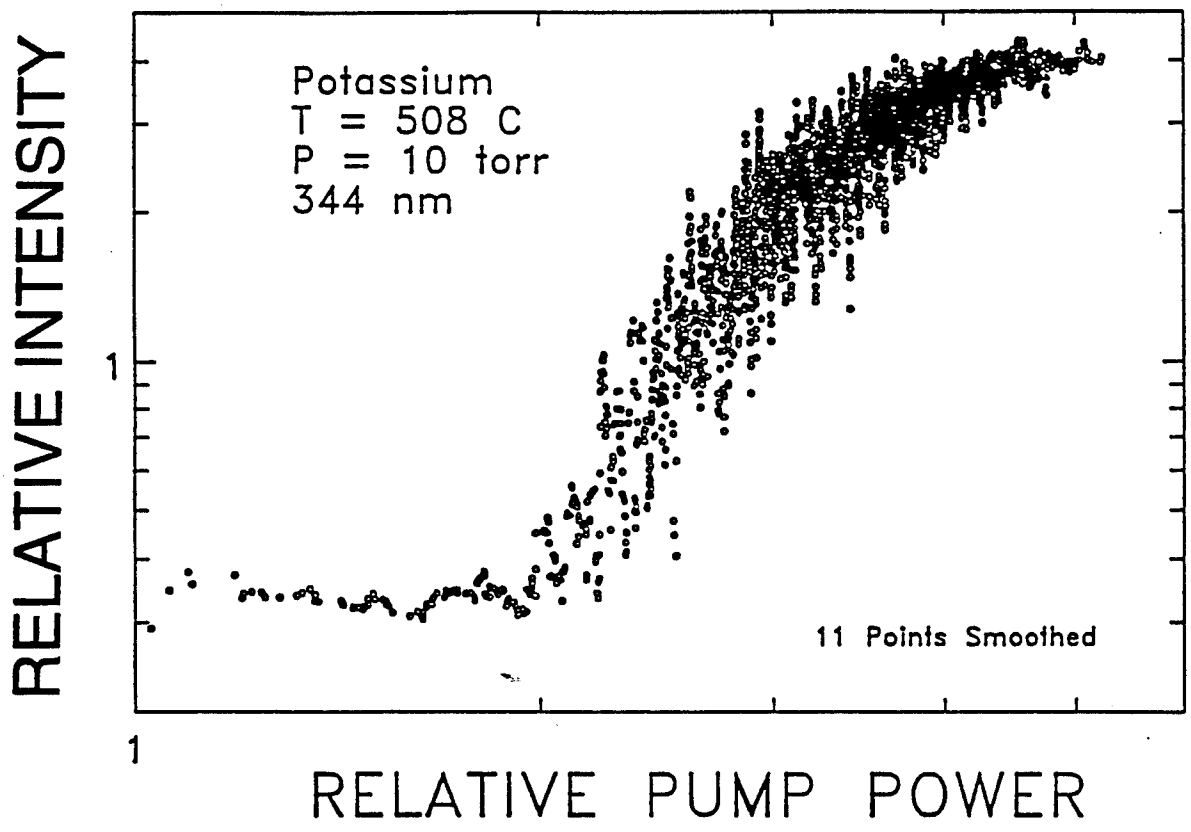

Figure 22 Variation of output pulse energy at 344 nm with the energy of the red (~625 nm) femtosecond pulses. Note the sharp onset of oscillation and rapid saturation of the UV energy.

These results are exciting for several reasons. The first is that several UV wavelengths can be produced efficiently from a single pump wavelength owing to the large peak intensities available from femtosecond laser systems. Secondly, since the pump pulse width is $<< T_2$ for the non-linear medium, the dynamics of generating the coherent UV and the characteristics of the output beam will differ markedly from the results that were obtained in the past with nanosecond pulses. Although these experiments are in the early stages, it is clear that this approach offers an attractive means for generating UV femtosecond pulses. Preliminary experiments with rubidium vapor have yielded similar results (but with shorter output wavelengths) and we intend to pursue this approach further by using excimer laser photodissociation of alkali-halide vapor. In this way, large number densities ($> 10^{14}$ cm^{-3}) of alkali atom excited species can be produced and one- and two-photon excitation of still higher-lying states will be an effective means for efficiently producing deep UV and VUV radiation.